

# Noise considerations in the determination of diffusion tensor anisotropy

Stefan Skare<sup>a,b,\*</sup>, Tie-Qiang Li<sup>c</sup>, Bo Nordell<sup>a,b</sup>, Martin Ingvar<sup>a</sup>

<sup>a</sup>MR Center, Karolinska Institute, Stockholm, Sweden

<sup>b</sup>Dept. of Medical Radiation Physics, Karolinska Institute, Stockholm, Sweden

<sup>c</sup>Department of Radiology, Stanford University, Stanford, CA 94305, USA

Received 2 January 2000; accepted 4 May 2000

## Abstract

In this study the noise sensitivity of various anisotropy indices has been investigated by Monte-Carlo computer simulations and magnetic resonance imaging (MRI) measurements in a phantom and 5 healthy volunteers. Particularly, we compared the noise performance of indices defined solely in terms of eigenvalues and those based on both the eigenvalues and eigenvectors. It is found that anisotropy indices based on both eigenvalues and eigenvectors are less sensitive to noise, and spatial averaging with neighboring pixels can further reduce the standard deviation. To reduce the partial volume effect caused by the spatial averaging with neighboring voxels, an averaging method in the time domain based on the orientation coherence of eigenvectors in repeated experiments has been proposed. © 2000 Elsevier Science Inc. All rights reserved.

*Keywords:* Diffusion tensor imaging; Anisotropy index; Noise sensitivity

## 1. Introduction

The self-diffusion anisotropy phenomenon has been used to obtain microstructure and physiological information of living tissues. For example, MRI measurement of diffusion anisotropy of water in the brain can map the orientations of the white matter fiber tracts [1–6] and disease induced abnormalities [7–10]. Other clinical applications include studying the ordered structure of muscle fibers [11] and the medulla of the kidney [12]. Different definitions of diffusion anisotropy indices have been introduced in the literature [13–19]. The anisotropy index determined from the ratio of the apparent diffusion coefficients (ADC) along the axes of the laboratory frame ( $x$ ,  $y$ , and  $z$ ) is rotationally variant and underestimates the diffusion anisotropy when the axes of the laboratory frame do not coincide with the principle directions of the diffusion tensor ( $\mathbf{D}$ ). The diffusion tensor and its eigenvalues can be determined by diffusion-weighted MRI with the diffusion weighted gradients applied in at least six non-collinear directions. Anisotropy indices based on eigenvalues and eigenvectors are rotationally invariant and can be compared between different regions, subjects, and physiological states.

Diffusion-weighted MRI has limited signal-to-noise ratio (SNR). For accurate assessment of the diffusion anisotropy, it is, therefore, important to optimize the experimental conditions and use an anisotropy measure that is robust to experimental noise. Previous studies have shown that diffusion anisotropy indices differ significantly in accuracy and noise sensitivity [16,20–22]. The results from a recent study by Papadakis et al. [20] indicate that noise sensitivity, contrast, and resolution are distinctive even for the same class of rotationally invariant anisotropy indices. Different approaches have been taken to reduce the noise sensitivities of anisotropy indices. Ulug and van Zijl [18] proposed a set of rotationally invariant indices determined directly from the orientation-dependent diffusion tensor elements without matrix diagonalization. Martin et al. [21] used orientation coherence of eigenvectors to reduce sorting bias. Based on simulation and phantom results, Bastin et al. [22] suggested that rotationally variant indices are always more favorable than rotationally invariant counterparts at low SNR. However, Pierpaoli and Basser [16] have shown previously that rotationally variant indices could severely underestimate the degree of diffusion anisotropy in vivo where diffusion tensor orientations are different in various regions. They have also proposed using spatial averages of inner products between diffusion tensors in neighboring voxels to derive an intervoxel lattice index that is a more robust rotationally

\* Corresponding author. Tel.: +46-8-517-761-18; fax: +46-8-517-732-66.

E-mail address: stefan@mrc.ks.se (S. Skare).

Table 1  
A list of anisotropy indices with definitions, literature sources, and value ranges

Index	Definition	Ref.	Value Range
$A_{xyz}$	$\frac{\max\{ADC_x, ADC_y, ADC_z\}}{\min\{ADC_x, ADC_y, ADC_z\}}$	1,2	$[1, \infty]$
$A_{ratio}$	$\lambda_1/\lambda_3$	13	$[1, \infty]$
$A_{ratio,m2}$	$\frac{\lambda_1}{(\lambda_2 + \lambda_3)/2}$	13	$[1, \infty]$
$A_{major}$	$\frac{\lambda_1 - (\lambda_2 + \lambda_3)/2}{3\bar{\lambda}}, \bar{\lambda} = (\lambda_1 + \lambda_2 + \lambda_3)/3$	14	$\{0,1\}$
$A_\sigma$	$\frac{1}{\sqrt{6\bar{\lambda}}} \sqrt{\sum_{i=x,y,z} (D_{ii} - \bar{\lambda}) + 2(D_{xy}^2 + D_{xz}^2 + D_{yz}^2)}$	14	$[0,1]$
$RA$	$\frac{1}{\sqrt{3}} \frac{\sqrt{\sum_{i=1,2,3} (\lambda_i - \bar{\lambda})^2}}{\bar{\lambda}}$	17	$[0, \sqrt{2}]$
$FA$	$\sqrt{\frac{\sum_{i=1,2,3} (\lambda_i - \lambda^-)^2}{\frac{3}{2} \sum_{i=1,2,3} \lambda_i^2}}$	17	$[0,1]$
$VR$	$\lambda_1 \lambda_2 \lambda_3 / \bar{\lambda}^3$	16	$[1,0]$
$A_{dd}$	$A_{dd} = \frac{\mathbf{D}_{ref} : \mathbf{D}_n}{\mathbf{D}_{ref} : \mathbf{D}_n}$ $\mathbf{D}_{ref} : \mathbf{D}_n = \sum_{k=1}^3 \sum_{s=1}^3 \lambda_{ref,s} \lambda_{n,k} (\mathbf{e}_{ref,s}^T \mathbf{e}_{n,k})^2$ $\mathbf{D}_{ref} : \mathbf{D}_n = \mathbf{D}_{ref} : \mathbf{D}_n - \frac{1}{3} \text{Trace}(\mathbf{D}_{ref}) \text{Trace}(\mathbf{D}_n)$	16,23	$\left[0, \frac{2}{3}\right]$
$LI$	$LI = \frac{\sum_{n=1}^8 a_n LI_n}{\sum_{n=1}^8 a_n}$ $LI_n = \sqrt{\frac{3}{8}} \frac{\sqrt{\mathbf{D}_{ref} : \mathbf{D}_n}}{\sqrt{\mathbf{D}_{ref} : \mathbf{D}_n} r_{IX}} + \frac{3}{4} \frac{\mathbf{D}_{ref} : \mathbf{D}_n}{\sqrt{\mathbf{D}_{ref} : \mathbf{D}_{ref}} \sqrt{\mathbf{D}_n : \mathbf{D}_n}}$	16,23	$[0,1]$

invariant index. In the present study, we have further investigated the noise sensitivities of different anisotropy indices with focus on comparing noise performances between indices based solely on eigenvalues (referred to as eigenvalue indices) and those defined both in terms of eigenvalues and eigenvectors (referred to as eigenvector indices). We have also proposed a time domain averaging method which takes advantage of the orientation coherence of eigenvectors in repeated experiments to reduce the possible partial volume effect caused by spatial averaging.

## 2. Theory

### 2.1. Background

A list of diffusion anisotropy indices proposed in the literature is compiled in Table 1, which includes definitions,

literature resources, and dynamic ranges. Sorted by their dynamic value ranges, diffusion anisotropy indices can be divided into IVR (infinite value range) and DVR (definite value range) groups.  $A_{xyz}$  is based on the ratio of  $ADC_k$  ( $k = x, y, z$ ) measured along the axis of the laboratory frame and is a rotationally variant index. The rotationally invariant indices can be further classified into indices defined solely in terms of the eigenvalues ( $\lambda_1, \lambda_2, \lambda_3$ ) and indices based on both the eigenvalues and eigenvectors ( $\hat{\mathbf{e}}_1, \hat{\mathbf{e}}_2$  and  $\hat{\mathbf{e}}_3$ ) of the diffusion tensor ( $\mathbf{D}$ ). The lattice index,  $LI$ , based on both eigenvalues and eigenvectors of the diffusion tensor is intervoxel in nature. It was introduced by Basser and Pierpaoli [16] to improve the accuracy of anisotropy estimates by taking the advantage of the orientational coherence of diffusion tensors in neighboring voxels. It has been demonstrated that the lattice index is less sensitive to noise than

other indices. However, it is not clear whether this is simply due to spatial averaging between the neighboring voxels (8 adjacent voxels) or the intrinsic characteristics associated with the inclusion of eigenvectors. To separate the spatial averaging effect from the intrinsic noise sensitivity, we consider the basic element,  $\mathbf{D}:\mathbf{D}'\mathbf{D}:\mathbf{D}'$ , of the lattice index as an independent anisotropy measure,  $A_{dd}$ . Its definition is specified in Table 1 and references [16,23]. Similar to the definition of  $LI$ , its corresponding spatially averaged version,  $A_{dd}^8$ , is defined as

$$A_{dd}^8 = \frac{\sum_{i=1}^8 a_i A_{dd}}{\sum_{i=1}^8 a_i} \quad (1)$$

where  $a_i = \sqrt{2}$  for diagonally located neighbors and 1 otherwise. To compare the noise performances between  $A_{dd}$  and  $A_{dd}^8$ , both indices were simulated separately.

## 2.2. Time-domain anisotropy index

The lattice indices,  $LI$  and  $A_{dd}^8$ , are weighted means of all adjacent neighbors and the corresponding anisotropy index maps are inevitably spatially low-pass filtered. To reduce partial volume effect induced by spatial averaging, eigenvector coherence in the time domain can be used instead. Similar to the orientation coherence of the diffusion tensors in the neighboring voxels, the direction estimates of the diffusion ellipsoid in a particular voxel measured at different time points would be correlated with each other, if the voxel is located in a region of anisotropy. On the other hand, in a voxel where the diffusion process is isotropic and differences in the measured eigenvalues result solely from random noise, we would expect that the eigenvectors measured at different time points are uncorrelated. To improve the estimate of diffusion anisotropy in a certain voxel without compromising the spatial resolution, we propose time domain averaging that incorporates coherence of the eigenvectors from repeated measurements. This requires at least two repeated measurements. Let  $\mathbf{D}_{\text{ref}}$  and  $\mathbf{D}'_{\text{ref}}$  represent, respectively, the diffusion tensor and its deviatoric measured at a reference time point, and  $\mathbf{D}_t$  and  $\mathbf{D}'_t$  be the diffusion tensor and its corresponding deviatoric estimated in a replicate experiment for the same voxel. A time domain lattice index,  $A_{ddt}$ , can be similarly defined as the intervoxel lattice index. The index is

$$A_{ddt} = \frac{\mathbf{D}_{\text{ref}}:\mathbf{D}'_t}{\mathbf{D}_{\text{ref}}:\mathbf{D}'_t} \quad (2)$$

If  $N$  repeated experiments are performed, an average time domain lattice index,  $A_{ddt}^N$ , can be defined as

$$A_{ddt}^N = \frac{\sum A_{ddt}}{N} \quad (3)$$

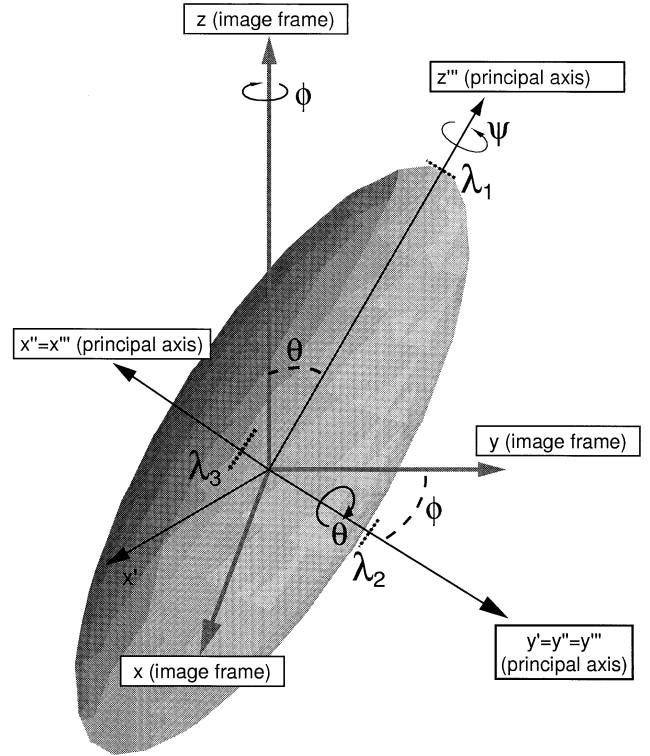


Fig. 1. The “rice”-shaped diffusion ellipsoid and its rotation coordinates with respect to the laboratory frame.

If the noise in  $A_{ddt}$  can be approximated as Gaussian distributed, the SNR for  $A_{ddt}^N$  is expected to be improved by a factor of  $\sqrt{N}$ .

## 3. Materials and methods

### 3.1. Simulations

The influence of noise on the estimates of anisotropy indices was studied by Monte Carlo computer simulation at different degrees of anisotropy and orientations (specified by the rotation angles  $\psi$ ,  $\phi$  and  $\theta$ ) for the “rice” shaped diffusion tensor ellipsoid (Fig. 1). Due to the axial symmetry of the “rice” shaped diffusion ellipsoid, the rotation angle,  $\psi$ , was set to zero in the simulations. The following orientations were simulated:  $\psi/\phi/\theta = 0^\circ/0^\circ/0^\circ$ ,  $0^\circ/30^\circ/15^\circ$ ,  $0^\circ/170^\circ/60^\circ$ , and  $0^\circ/60^\circ/0^\circ$ . For each orientation, the ratio  $\lambda_1/\lambda_2$  was varied from 1 to 10 with an increment of 1, while keeping the ratio at  $\lambda_2/\lambda_3 = 1$ . The average eigenvalue  $\bar{\lambda} = (\lambda_1 + \lambda_2 + \lambda_3)/3$  was kept to a constant value of  $1.0 \times 10^{-9} \text{m}^2/\text{s}$  for all the simulations.  $\bar{\lambda}$  was chosen to be in agreement with typical values of the experimental measurement for normal cerebral tissue. A simulation started by assigning the eigenvalues of the diffusion tensor and involved recalculation of the eigenvalues and eigenvectors after introducing various levels of random noise to the diffusion-weighted images.

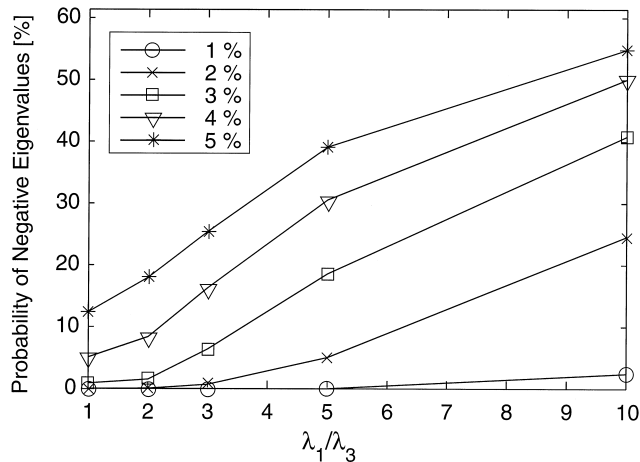


Fig. 2. The probability of obtaining negative eigenvalues for the 'rice' shaped diffusion tensor as a function of  $\lambda_1/\lambda_3$  at different noise levels (1–5% of  $S_0$ ).

For each degree of anisotropy and orientation the following simulation procedures have been performed. [1] The diffusion tensor in the principal coordinate was defined by assigning the eigenvalues to the diagonal elements of a  $3 \times 3$  diagonal matrix ( $\mathbf{D}_{\text{diag}}$ ). Its representation,  $\mathbf{D}$ , in the laboratory frame was obtained by applying the rotation matrix associated with the orientation to the diagonal matrix. [2] The six ADC values along the directions defined by the diffusion tensor imaging scheme were determined from the tensor components,  $D_{ij}$ , in the laboratory frame and the diffusion weighted signal intensities,  $S_0$  and  $S_b$ , corresponding to 2 different  $b$  values (0 and 900  $\text{s/mm}^2$ ) were computed from the known ADC and  $b$  values. [3] Gaussian distributed random noise between 1 and 10% (relative to the signal intensity at  $S_0$  at  $b = 0$ ) were added to the real and imaginary parts of the signal. Four different noise levels (1, 3, 5, and 10% of  $S_0$ ) were simulated with corresponding SNR of 70.7, 23.6, 14.1 and 7.1 for  $S_0$ , respectively. Noise perturbed signal intensities were used to recalculate the noise affected ADC values. [4] The diffusion tensor components,  $D_{ij}$ , eigenvalues and eigenvectors were recalculated from the noise affected ADC values. [5] Anisotropy indices listed in Table 1 and Eqs. 1–3 were estimated according to their respective definitions using the noise perturbed parameters (eigenvalues and eigenvectors) of the diffusion tensor. The related mathematical details of the above procedures are given in the Appendix. At each noise level  $10^5$  replicate simulations were performed and statistical analysis of the data included evaluations of the probability of obtaining negative eigenvalues, the distribution of the eigenvalues, and average bias and standard deviation (SD) of each anisotropy index. To facilitate comparison among DVR indices,  $RA$ ,  $A_{\text{dd}}$ ,  $A_{\text{dd}}^8$ ,  $A_{\text{ddt}}$  and  $A_{\text{ddt}}^N$  were rescaled appropriately so that these indices also have the dynamic range from 0 to 1. Although it is desirable to compare the noise sensitivity in terms of relative bias (bias/anisotropy), it is difficult in practice to evaluate the relative bias of the DVR

indices in the near isotropy and weak anisotropy range. Any finite bias can produce a value of infinity for the relative bias.

### 3.2. Phantom study

The purpose of the phantom study was to examine the false positive anisotropy effect in the case of isotropy at an SNR close to the in vivo situation. The various anisotropy indices of a water phantom were measured experimentally using diffusion weighted MRI and the deviations from the true isotropy were used to evaluate the noise sensitivity of these indices. A spherical water phantom (with a radius of 9 cm) doped with  $\text{CuSO}_4$  ( $\text{ADC} = 2.2 \times 10^{-3} \text{ mm}^2/\text{s}$ ) was measured on a 1.5T GE Signa Echo-speed MRI scanner (Milwaukee, WI, USA). A single-shot diffusion-weighted spin-echo echo-planar imaging (SE-EPI) pulse sequence was implemented for the self-diffusion measurements. For the diffusion tensor imaging, a set of gradient combinations including the tetrahedral set [14,15] and two other gradient directions ( $g_x, g_y, 0$ ) and ( $g_x, 0, g_z$ ) were used. Diffusion-weighted images were acquired at two different  $b$  values (0 and 500  $\text{s/mm}^2$ ) using  $\text{TE/TR} = 90/1000$  ms. A single slice was acquired across the center of the phantom using a FOV of 22 cm, matrix size of  $128 \times 128$  and slice thickness of 4 mm. In order to perform time domain averaging and estimate the time-domain lattice indices,  $A_{\text{ddt}}$  and  $A_{\text{ddt}}^N$ , 8 replicate measurements were also performed ( $N = 8$ ). The standard deviation of the signal intensity at  $b = 0$  was approximately 5%.

### 3.3. Human study

Maps of the various anisotropy indices in the human brain were measured experimentally and the quality differences of these anisotropy index maps should provide a qualitative in vivo validation of the results from the simulations and phantom studies. Five healthy volunteers (4 male, 1 female, aged 27–46) were measured. For each subject 5–10 axial slices covering the corpus callosum were imaged using the SE-EPI pulse sequence on a 3T LX medical MRI scanner (General Electric, Milwaukee, WI, USA). The essential data acquisition parameters used were  $b$  value = 1000  $\text{s/mm}^2$ ,  $\text{TE/TR} = 81/6000$  ms, matrix size of  $128 \times 128$ , FOV of 22 cm, slice thickness of 5 mm. The diffusion tensor mapping scheme was the same as that used for the phantom measurements and simulations. 4–8 replicate scans were performed to allow the estimate of the time-domain lattice index,  $A_{\text{ddt}}^N$ . To reduce the possible motion artifacts between different measurements image registrations were also performed. The auxiliary program, *im-reg*, included in the functional MRI software AFNI [24–26] was used for image registration, which minimizes the mean squared error between the selected reference image and the images to be registered.

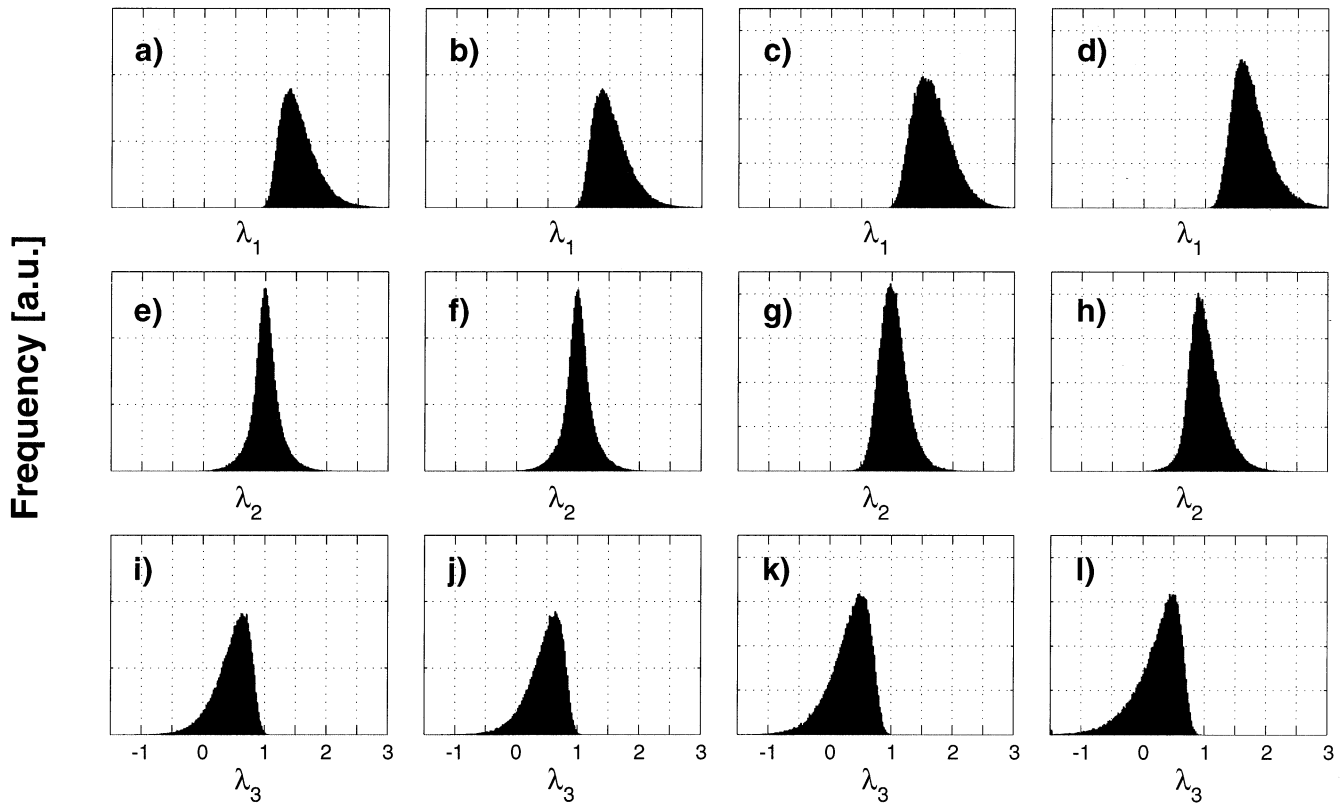


Fig. 3. Distribution histograms of eigenvalues as a function of anisotropy and tensor orientation. (a) isotropic diffusion ( $\lambda_1/\lambda_2/\lambda_3 = 1$ ) at collinear  $\psi/\theta/\phi = 0^\circ/0^\circ/0^\circ$  orientation, (b) isotropic diffusion at non-collinear  $\psi/\theta/\phi = 0^\circ/30^\circ/15^\circ$  orientation, (c) anisotropy diffusion tensor ( $\lambda_1/\lambda_2/\lambda_3 = 2:1:1$ ) at collinear  $\psi/\theta/\phi = 0^\circ/0^\circ/0^\circ$ , and (d) anisotropy diffusion tensor at non-collinear  $\psi/\theta/\phi = 0^\circ/30^\circ/15^\circ$ . The simulated noise level was 5% of  $S_0$ . The eigenvalue distributions are rotational invariant in the isotropic case (a and b). The invariance is not always valid for anisotropy diffusion (b and c).

## 4. Results

### 4.1. Simulations

In Fig. 2 the probability of obtaining negative eigenvalues is shown as a function of  $\lambda_1/\lambda_3$  at different noise levels (1–5%). The probability of obtaining negative eigenvalues increases with the degree of diffusion anisotropy and the noise level. Fig. 3 shows the eigenvalue distributions at a noise level of 5% for isotropic ( $\lambda_1/\lambda_2/\lambda_3 = 1$ , Fig. 3, a and b) and anisotropic ( $\lambda_1/\lambda_2/\lambda_3 = 2/1/1$ , Fig. 3, c and d) diffusion tensors. For isotropic diffusion, coordinate rotation has no effect on the distribution of the eigenvalues, and the distributions of the magnitude sorted eigenvalues are identical for different orientations (Fig. 3, a and b). Corresponding data for the anisotropic diffusion (Fig. 3, c and d) demonstrate that the distributions of the eigenvalues are dependent on the relative tensor orientation in the laboratory frame. In the presence of noise, the eigenvalue distributions for anisotropy diffusion tensors start to deviate from the intrinsic rotational invariance. Fig. 3 also shows that sorting the eigenvalues in descending order ( $\lambda_1 > \lambda_2 > \lambda_3$ ) gives rise to significant overestimation of  $\lambda_1$  and underestimation of  $\lambda_3$ .

Fig. 4 shows the bias (Fig. 4, a–c) and SD (Fig. 4, d–f) of various anisotropy indices for the “rice”-shaped diffusion

tensor as a function of  $\lambda_1/\lambda_3$  at the noise level of 3% and the orientation angles of  $\psi/\phi/\theta = 0^\circ/30^\circ/15^\circ$ . At the same noise level, the bias and SD are significantly different for the various indices indicating different degrees of sensitivity to noise. In the IVR index group (Figs. 4a and d), the rotationally variant index  $A_{xyz}$  has the lowest bias and variance, whereas the rotationally invariant index,  $A_{ratio}$ , is most susceptible to noise (Fig. 4, a and d). In the DVR group, the indices based on both eigenvalues and eigenvectors (Fig. 4, c and f) are generally more robust than the eigenvalue indices (Fig. 4, b and e).  $A_{ddt}^1$  and  $A_{ddt}^8$  have the lowest bias in the low anisotropy range ( $\lambda_1/\lambda_3 < 2$ ), while the lattice indices,  $LI_n$  and  $LI$ , perform best in the higher anisotropy range ( $\lambda_1/\lambda_3 > 2$ ). The standard deviations for  $LI$  and  $A_{ddt}^8$  are lower than those of the corresponding non-averaged elements  $LI_n$  and  $A_{ddt}^1$  (Fig. 4f). It is evident that the eigenvector indices have the intrinsic characteristics of low bias and that spatial averaging with neighboring voxels can further reduce their standard deviations. Among the eigenvalue based indices,  $A_{major}$  has the lowest bias in the entire anisotropy range.  $FA$  has the highest bias and SD in the low anisotropy range. The noise performance of  $RA$  is intermediate in the low anisotropy range but worst in the high anisotropy range. Unlike the other DVR indices both the

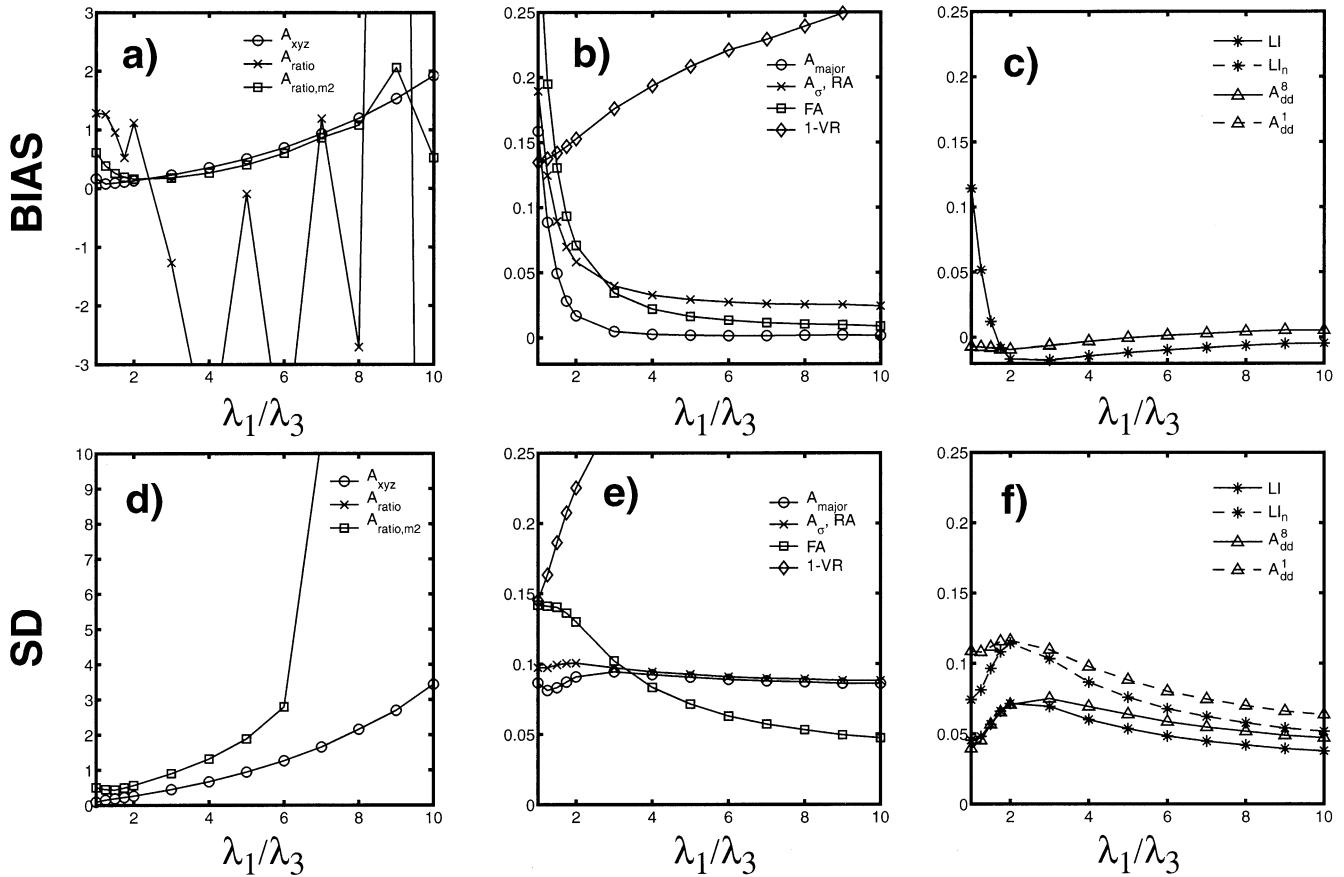


Fig. 4. The bias (a-c) and SD (d-f) as a function of  $\lambda_1/\lambda_3$ . The results for the “rice” shaped diffusion ellipsoid with orientation  $\psi/\theta/\phi = 0^\circ/30^\circ/15^\circ$  are shown. The biases were the mean value difference of anisotropy indices between the noise levels of 0 and 3%. The results were sorted into IVR (a,d) and DVR (b, c, e, f) groups. The DVR group was further separated into eigenvalue (c, d) and eigenvector indices (e, f). The eigenvalue indices are only dependent on the eigenvalues of the diffusion tensor. The eigenvector indices are defined both in terms of eigenvalues and eigenvectors of the diffusion tensor.

bias and SD of the “1-VR” index increase with the degree of anisotropy.

#### 4.2. Experimental verification

Fig. 5 shows the phantom data for various indices. The average values  $\pm$  SD were obtained from a region of interest (ROI) chosen in the center of the phantom image containing approximately 5000 pixels. The experimental results for the isotropic water phantom agree very well with the simulation data. As shown in Fig. 5a,  $A_{xyz}$  is the best IVR measure for the isotropic medium, whereas  $A_{ratio}$  produces highest false positive anisotropy and variance. Among the eigenvalue indices, FA has the highest bias and VR has the highest SD (Fig. 5b). As shown in Fig. 5c, the eigenvector indices have the lowest false positive anisotropy for an isotropic medium. Both spatial and time domain averaging can reduce variances of anisotropy indices.

The results from all volunteers showed the same trend and a representative set of anisotropy index maps from the human study is shown in Fig. 6. Nine different index maps calculated from the same experimental data set are shown. The quality of these index maps are directly related to their

noise sensitivity. For fair comparison, all the maps were based on average results of 4 repeated measurements. It is clear that  $A_{ratio}$  has the worst quality in the IVR index group (top row). The noise level of the  $A_{xyz}$  map is low, but it depicts very little anisotropy. Among the DVR index maps, the eigenvector indices,  $LI$  and  $A_{dd}^8$ , have the highest quality. Compared with these spatially averaged indices, the time domain averaged index,  $A_{dd}^4$ , has somewhat higher noise level and is less smooth. Like the eigenvalue indices (middle row), more local variations are observable in  $A_{dd}^4$ . Furthermore, it detects some small regions of very high anisotropy that are only partially observable in the eigenvalues index maps but are completely absent in the  $LI$  and  $A_{dd}^8$  index maps. For example, in the  $A_{dd}^4$  map there are the two bright circular regions located close to the genu of the internal capsule next to the midline that are very likely to be the fornix columns. In the eigenvalue index maps,  $FA$  depicts comparatively high anisotropy in the more isotropic regions of the brain and has the poor contrast.  $VR$  is prone to more noise but shows higher contrast between isotropic and anisotropic regions. The  $RA$  map has intermediate contrast and noise level.

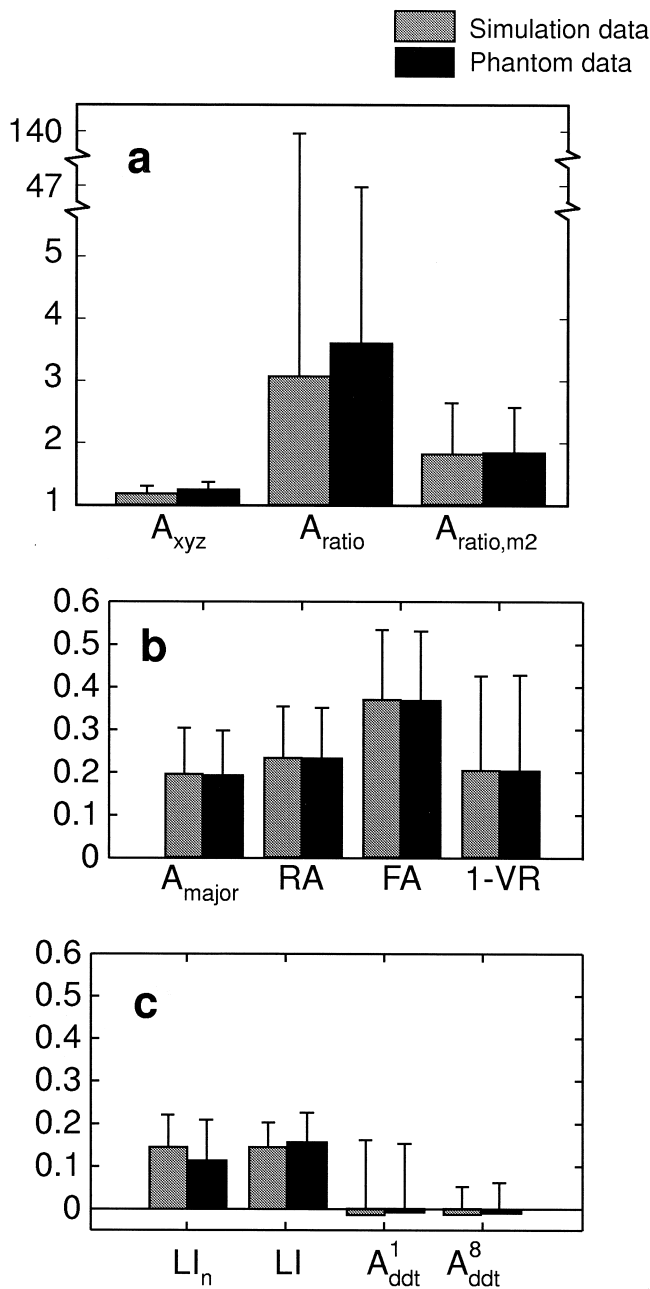


Fig. 5. Experimentally measured (gray bars) anisotropy indices  $\pm$  SD for an isotropic water phantom. The results for a ROI of approximately 5000 pixels are grouped into IVR indices (a), DVR indices based on eigenvalues (b), and DVR indices defined by eigenvalues and eigenvectors (c). To facilitate comparison the corresponding simulation results (black bars) are also shown. The SD of the MRI signal intensity of  $S_0$  was approximately 5%, which matched the noise level used for the simulations.

## 5. Discussion

### 5.1. Negative eigenvalues and sorting bias

Results from the computer simulations indicate that the probability of obtaining negative eigenvalues increases as the noise level and the degree of anisotropy increase. Neg-

ative eigenvalues give rise to erroneous anisotropy measure. If negative eigenvalues are inappropriately filtered, biased diffusion anisotropy will be obtained. Isotropic structures can appear anisotropic and structures with low anisotropy depict higher degree of anisotropy. In practical anisotropy mapping it is, therefore, desirable to optimize SNR and diminish the probability of having negative eigenvalues. Besides hardware improvements, it is preferable to use diffusion tensor imaging schemes that are less sensitive to error propagation.

It is well known that system noise introduces sorting bias into anisotropy indices when eigenvalues of the diffusion tensor are ordered according to their magnitude [16,20,21]. Sorting bias artificially increases the difference between the minimum and maximum eigenvalues and results in elevated anisotropy of isotropic and weakly anisotropic media. The simulation results from the present study also demonstrate that the sorting bias is profound both for isotropic and anisotropic media. For the worst case scenario of an isotropic medium, the sorted eigenvalue distributions are significantly different from each other, although the true values should be the same (see Fig. 3, a, b, e, f, i, and j). The undesirable effect of sorting on the anisotropy index,  $A_{ratio} = \lambda_1/\lambda_3$ , is also experimentally evident. As shown in the phantom data (Fig. 5a), at the noise level of 5%,  $A_{ratio}$  was overestimated by a factor of more than 3. Systematic errors of such an extend greatly limit the use of the indices which depend on eigenvalue sorting. A polynomial sorting method taking advantage of local fiber directional coherence has recently been proposed by Martin et al. [21] to reduce sorting bias in weakly anisotropy media.

### 5.2. Deviations from rotational invariance

In principle, anisotropy indices based on the eigenvalues of the tensor are rotationally invariant for all diffusion ellipsoid shapes, orientations and degrees of anisotropy. In the noise free situation, the determination of eigenvalues is independent of the relative orientation between the principle axis of the diffusion tensor and the directions of the diffusion weighted gradients. The diagonalization of the diffusion tensor should always produce the same set of eigenvalues irrespective to the orientation of the tensor in the laboratory frame. As demonstrated by differences in eigenvalue distributions for the same diffusion tensor at two different orientations (Fig. 3, c, d, g, h, k, and l), at limited SNR the evaluated eigenvalues for anisotropy diffusion may deviate from the rotational invariance. In the absence of noise, the tensor presentation in the laboratory frame is directly related to the eigenvalues by the rotation matrix, and the column vectors of the rotation matrix are the eigenvectors. Different orientations simply give rise to different rotation matrices and eigenvectors. In the presence of noise, the diagonalization of the error perturbed data cannot be completed with the original rotation matrix. A complete re-factorization of the error-superimposed matrix will result

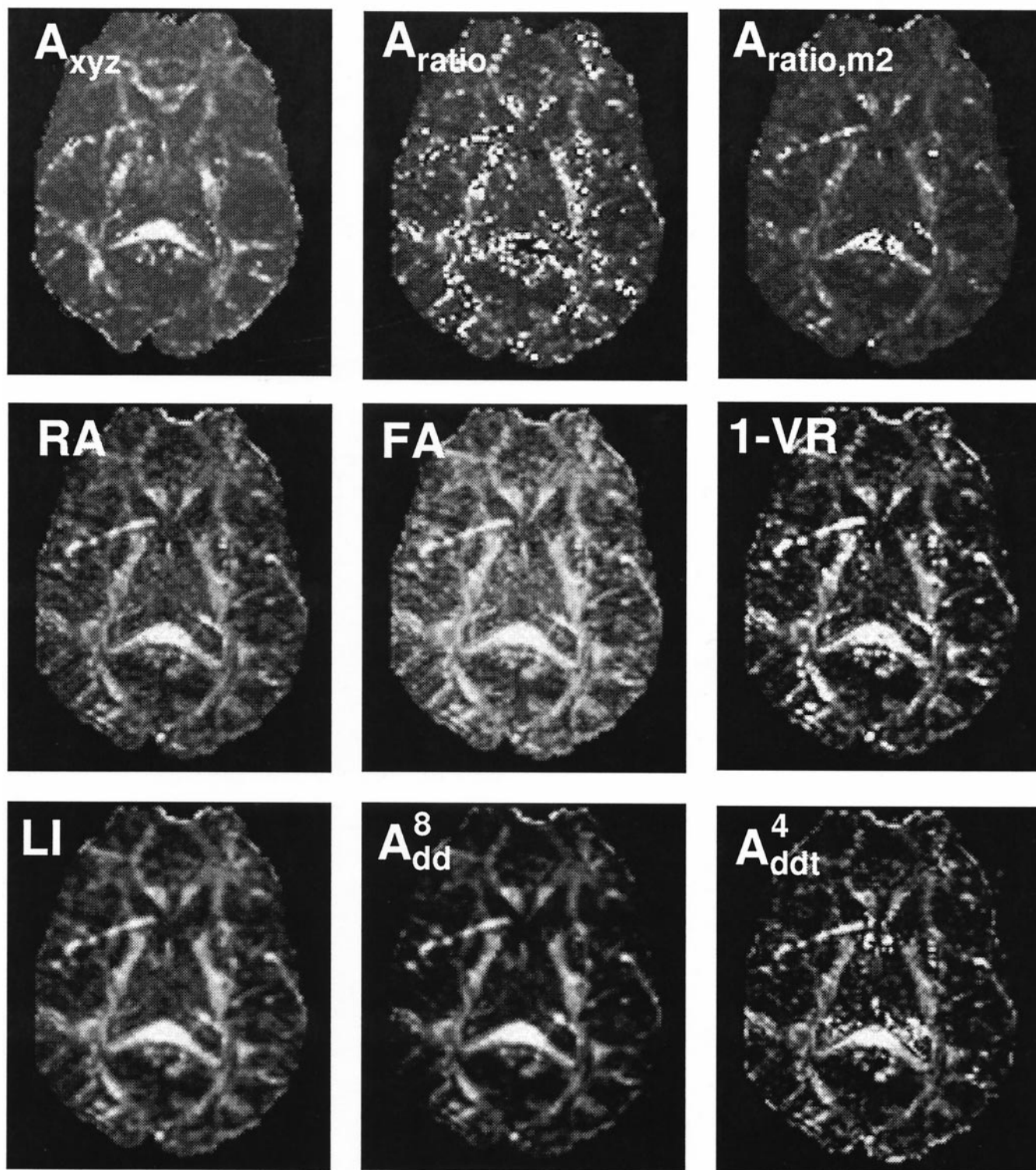


Fig. 6. A representative set of anisotropy index maps measured in a normal subject using a spatial resolution of  $1.7 \times 1.7 \times 5 \text{ mm}^3$ , TE/TR = 81/6000, two  $b$  values (0 and  $900 \text{ s/mm}^2$ ) and 4 replicates. Three IVR (top row) indices, DVR eigenvalue indices (middle row) and DVR eigenvector indices (bottom row) are shown.

in a new set of eigenvalues and eigenvectors that are somewhat different from the true values. It is expected that the choice of diffusion tensor imaging schemes will influence the rotational invariance of an anisotropy index. A tensor

imaging scheme consists of a finite number of diffusion-weighted gradient directions. The limited number of data sampling along a few non-uniformly distributed directions can result in orientation dependent noise propagation.

### 5.3. Eigenvalue indices

The results for the noise performance of IVR indices from the simulations and experimental investigations of the phantom and human brains are very consistent.  $A_{\text{ratio}}$  is the most susceptible to noise (high bias and SD) apparently due to the sorting bias discussed above. The variance of  $A_{\text{xyz}}$  is low and its bias for isotropy is also small, but the  $A_{\text{xyz}}$  map of the human brain shows very little contrast between gray and white matter.  $A_{\text{xyz}}$  is directly calculated from the ADC ratios and any diffusion tensor that is not collinearly oriented with the diffusion-weighted gradient is inevitably underestimated. Previous studies [16,22] based on other diffusion tensor imaging schemes had similar findings. The rotational variance of  $A_{\text{xyz}}$  precludes its use for any quantitative measurement of diffusion anisotropy in the brain.

In a recent study by Papadakis et al. [20], it was reported that noise performances of the same class eigenvalues indices,  $FA$ ,  $RA$ , and  $VR$ , are significantly different. The results from the present study also support such a notion, although different diffusion tensor imaging schemes and simulation approaches were used. For most of the DVR eigenvalue indices ( $A_{\text{major}}$ ,  $RA$ , and  $FA$ ) both the bias and SD decrease with the degree of anisotropy, whereas the volume index,  $VR$ , shows the opposite trend. This observed behavior of  $VR$  index is somewhat contrary to the findings of previous studies [16,22]. According its definition [16], the  $VR$  index should be insensitive to the orientation of the tensor and is not affected by sorting of the eigenvalues. However, it involves a product term,  $\lambda_1\lambda_2\lambda_3$ , which makes it extremely sensitive to negative eigenvalues. We found that the bias and SD of the  $VR$  index behaved similarly as the other DVR eigenvalue indices after filtering the negative eigenvalue values.

### 5.4. Eigenvector indices and time domain averaging

Before the introduction of the intervoxel lattice index,  $LI$ , by Pierpaoli and Basser [16], diffusion anisotropy was essentially measured in terms of eigenvalues and the orientation information of the diffusion tensor was not incorporated into the anisotropy indices. As demonstrated by the present and previous [16] studies, eigenvector indices are generally more robust than the eigenvalue indices. From the comparison of the noise performances between  $LI_n$  and  $LI$ ,  $A_{\text{dd}}$  and  $A_{\text{dd}}^8$ , it is clear that the robustness of  $LI$  and  $A_{\text{dd}}^8$  is intrinsically associated with inclusion of eigenvector in the definitions. Spatial averaging of  $LI_n$  and  $A_{\text{dd}}$  with adjacent voxels merely reduces SD but not the bias (Figs. 4c and f). A similar low-pass filtering of eigenvalue indices, such as  $RA$  and  $FA$ , can also reduce the SD and obtain more smooth anisotropy index maps. Further insights into intrinsic properties of the eigenvector anisotropy indices can be acquired by comparing the noise performances between  $LI_n$  and  $A_{\text{dd}}$ .  $LI_n$  is approximately a square root version of  $A_{\text{dd}}$  but it has much higher false positive anisotropy in the near isotropy

range (Fig. 5c). A meaningful  $LI_n$  index value requires a non-negative  $A_{\text{dd}}$ . Selective filtering of the negative input values for the square root argument in  $LI_n$  inevitably overestimates the true anisotropy. In terms of low systematic bias,  $A_{\text{dd}}$  is the most robust index. As shown in Fig. 4c,  $A_{\text{ddt}}$  and  $A_{\text{ddt}}^8$  have very negligible bias in the near isotropy range. The experimental results from the isotropic phantom (Fig. 5c) further confirmed this. It should be pointed out in the case of isotropy, the results for  $A_{\text{dd}}$  and  $A_{\text{dd}}^8$  are exactly the same as those for  $A_{\text{ddt}}$  and  $A_{\text{ddt}}^8$ , respectively.

One of the potential advantages of using time domain averaging over spatial averaging as used in  $LI$  is that the assumption of local homogeneity of tensor direction field is not required. With time domain averaging, the loss of the eigenvector coherence is only the consequence of the random noise. Direction change on the spatial scale of voxel size due to anatomic structure changes has no impact on time domain averaging and smaller structures will not be filtered away. However, the various averaging strategies in the time domain, such as multi  $b$  values versus single  $b$  values with multi replicates, need to be further investigated in detail.

## 6. Conclusions

This study has demonstrated that in the assessment of diffusion anisotropy by MRI the choice of a robust anisotropy measure is of crucial importance. For quantitative comparison, a robust anisotropy index should be rotationally invariant. The rotational invariance of eigenvalue indices may not always be valid in the presence of noise. The indices based on both eigenvalues and eigenvectors, such as  $LI_n$  and  $A_{\text{dd}}$ , are more robust than the eigenvalue indices. Spatial averaging of  $LI_n$  and  $A_{\text{dd}}$  with adjacent voxels can further reduce their variances at the cost of increased partial volume effect. This can be remedied by using time-domain averaging.

## Acknowledgments

Stimulating discussions with Profs. G. H. Glover and M. E. Moseley have been helpful. The 3T MRI measurements were conducted at Lucas MRS Center, Department of Radiology, Stanford University. T. Q. Li was supported by NIH NCRR P-41 09784.

## Appendix: the simulation procedure

To study the effects of noise level on the accuracy of various diffusion anisotropy indices, we used Monte-Carlo simulation. The procedure and related mathematical details are given below.

(1) Defining a diagonal matrix,  $\mathbf{D}_{\text{diag}}$ , by assigning the

eigenvalues,  $\lambda_i$ , to its diagonal elements, where the anisotropy major axis was chosen to be the  $z'''$  axis.

$$\mathbf{D}_{diag} = \begin{bmatrix} \lambda_{x'''} & 0 & 0 \\ 0 & \lambda_{y'''} & 0 \\ 0 & 0 & \lambda_{z'''} \end{bmatrix} \quad (4)$$

In this paper the eigenvalues are denoted  $\lambda_1, \lambda_2$  and  $\lambda_3$ , with  $\lambda_1 = \lambda_2''', \lambda_2 = \lambda_{y'''}, \lambda_3 = \lambda_{z'''}$ .

The diffusion tensor representation in the laboratory frame,  $\mathbf{D}$ , is related to  $\mathbf{D}_{diag}$  by the rotation matrix,  $\mathbf{R}$ , which is defined by the rotation angles,  $\theta, \phi$ , and  $\psi$ . This is

$$\mathbf{D} = \mathbf{R}^T \mathbf{D}_{diag} \mathbf{R} \quad (5)$$

$$\mathbf{R} = \begin{bmatrix} \cos\psi & \sin\psi & 0 \\ -\sin\psi & \cos\psi & 0 \\ 0 & 0 & 1 \end{bmatrix} \begin{bmatrix} \cos\theta & 0 & -\sin\theta \\ 0 & 1 & 0 \\ \sin\theta & 0 & \cos\theta \end{bmatrix} \cdot \begin{bmatrix} \cos\phi & \sin\phi & 0 \\ -\sin\phi & \cos\phi & 0 \\ 0 & 0 & 1 \end{bmatrix} \quad (6)$$

Due to the symmetry of the diffusion tensor, only six of the nine elements,  $D_{ij}$ , need to be calculated. These are  $D_{xx}, D_{yy}, D_{zz}, D_{xy}, D_{xz}$ , and  $D_{yz}$ .

(2) The diffusion tensor imaging scheme to be simulated is defined by the following six gradient vectors,  $\hat{\mathbf{q}}_i$

$$\hat{\mathbf{q}}_1 = \frac{1}{\sqrt{3}} \begin{bmatrix} 1 \\ 1 \\ 1 \end{bmatrix}, \hat{\mathbf{q}}_2 = \frac{1}{\sqrt{3}} \begin{bmatrix} -1 \\ -1 \\ 1 \end{bmatrix}, \hat{\mathbf{q}}_3 = \frac{1}{\sqrt{3}} \begin{bmatrix} 1 \\ -1 \\ -1 \end{bmatrix}, \\ \hat{\mathbf{q}}_4 = \frac{1}{\sqrt{3}} \begin{bmatrix} -1 \\ 1 \\ -1 \end{bmatrix}, \hat{\mathbf{q}}_5 = \frac{1}{\sqrt{2}} \begin{bmatrix} 1 \\ 1 \\ 0 \end{bmatrix}, \hat{\mathbf{q}}_6 = \frac{1}{\sqrt{2}} \begin{bmatrix} 1 \\ 0 \\ 1 \end{bmatrix} \quad (7)$$

The  $ADC_i$  ( $i = 1, 2, \dots, 6$ ) value “sampled” in each direction is related to  $\mathbf{D}$  by

$$ADC_i = \hat{\mathbf{q}}_i^T \mathbf{D} \hat{\mathbf{q}}_i \quad (8)$$

From eq. 10, it is trivial to show that the measured ADC data,  $\mathbf{D}_m = [ADC_1, ADC_2, ADC_3, ADC_4, ADC_5, ADC_6]^T$  and the elements of the diffusion tensor  $\mathbf{D}_{elem} = [D_{xx}, D_{yy}, D_{zz}, D_{xy}, D_{xz}, D_{yz}]^T$  are related by the transformation matrix,  $\mathbf{A}$

$$\mathbf{D}_m = \mathbf{A} \mathbf{D}_{elem} \quad (9)$$

where

$$\mathbf{A} = \frac{1}{3} \begin{bmatrix} 1 & 1 & 1 & 2 & 2 & 2 \\ 1 & 1 & 1 & 2 & -2 & -2 \\ 1 & 1 & 1 & -2 & -2 & 2 \\ 1 & 1 & 1 & -2 & 2 & -2 \\ 3/2 & 3/2 & 0 & 1 & 0 & 0 \\ 3/2 & 0 & 3/2 & 0 & 1 & 0 \end{bmatrix} \quad (10)$$

Once the ADC is determined, the signal intensities of the diffusion weighted images,  $S_b$ , at different  $b$  values can be calculated according to the Stejskal-Tanner [27] equation:

$$S_b = S_0 e^{-n\gamma^2 \delta^2 G^2 (\Delta - \delta/3) ADC} = S_0 e^{-b ADC} \quad (11)$$

where  $n$  is the number of simultaneously applied diffusion encoding gradients;  $G, \delta$ , and  $\Delta$  are the amplitude, duration, and time offset of the diffusion encoding gradients, respectively.  $\gamma$  is the gyromagnetic constant for  $^1\text{H}$ .

(3) Gaussian distributed noise was superimposed on the real and imaginary part of  $S_b$  and the noise perturbed ADC values are evaluated by non-linear curve fitting of Eq. [13] to  $S_b$  at two different  $b$  values.

(4) The noise affected diffusion tensor elements,  $\mathbf{D}_{elem}$ , are calculated by reversing step 2.

$$\mathbf{D}_{elem} = \mathbf{A}^{-1} \mathbf{D}_m \quad (12)$$

The simulated eigenvalues and eigenvectors,  $\lambda_i$  and  $\hat{\mathbf{e}}_i$ , are obtained by numerically diagonalizing the noise perturbed diffusion tensor matrix,  $\mathbf{D}$ .

(5) Various anisotropy indices given in Table 1 and eqs. 1–3 are evaluated from the  $ADC$ , eigenvalues, and eigenvectors according to their definitions.

## References

- [1] Moseley ME, Cohen Y, Kucharczyk J, et al. Diffusion weighted MRI of anisotropic water diffusion in cat central nervous system. *Radiology* 1990;176:439–45.
- [2] Chenvert TL, Brunberg JG, Pipe JG. Anisotropic diffusion in human white matter: demonstration with MR techniques in vivo. *Radiology* 1990;177:401–5.
- [3] Doran M, Hajnal JV, van Bruggen N, et al. Normal and abnormal white matter tracts shown by MR imaging using directional diffusion weighted sequences. *J Comput Assist Tomogr* 1990;14:865–73.
- [4] Shimony JS, McKinstry RC, Akbudak E, et al. Quantitative diffusion-tensor anisotropy brain MR imaging: normative human data and anatomic analysis. *Radiology* 1999;212:770–84.
- [5] Xue R, van Zijl PC, Crain BJ, et al. In vivo three-dimensional reconstruction of rat brain axonal projections by diffusion tensor imaging. *Magn Reson Med* 1999;42:1123–7.
- [6] Virta A, Barnett A, Pierpaoli C. Visualizing and characterizing white matter fiber structure and architecture in the human pyramidal tract using diffusion tensor MRI. *Magn Reson Imaging* 1999;17:1121–33.
- [7] Buchsbaum MS, Tang CY, Peled S, et al. MRI white matter diffusion anisotropy and PET metabolic rate in schizophrenia. *Neuroreport* 1998;9:425–30.
- [8] Lim KO, Hedehus M, Moseley ME, et al. Compromised white matter tract integrity in schizophrenia inferred from diffusion tensor imaging. *Archives of General psychiatry* 1999;56:367–74.
- [9] Klingberg T, Vaidya CJ, Gabrieli JD, et al. Myelination and organization of the frontal white matter in children: a diffusion tensor MRI study. *Neuroreport* 1999;10:2817–21.
- [10] Neil JJ, Shiran SI, McKinstry RC, et al. Normal brain in human newborns: apparent diffusion coefficient and diffusion anisotropy measured by using diffusion tensor MR imaging. *Radiology* 1998;209:57–66.
- [11] Cleveland GG, Chang DC, Hazlewood CF, et al. Nuclear magnetic resonance measurement of skeletal muscle: anisotropy of the diffusion coefficient of intracellular water. *Biophys J* 1976;16:1043–53.
- [12] Muller MF, Prasad PV, Bimmler D, et al. Functional imaging of the kidney by means of measurement of the apparent diffusion coefficient. *Radiology* 1997;193:441–50.

- [13] Basser PUJ, Mattiello J, Le Bihan D. MR diffusion tensor spectroscopy and imaging. *Biophys J* 1994;66:259–67.
- [14] Conturo TE, McKinstry Rc, Akbudak E, et al. Encoding of anisotropic diffusion with tetrahedral gradient: a general mathematical diffusion formalism and experimental results. *Magn Reson Med* 1996;35:399–412.
- [15] Liu G, van Gelderen P, Moonen CTW. Single-shot diffusion MRI on a conventional clinical instrument. In: *Second SMR Meeting*, San Francisco, 1994. p. 1034.
- [16] Pierpaoli C, Basser BJ. Toward a quantitative assessment of diffusion anisotropy. *Magn Reson Med* 1996;36:893–906.
- [17] Basser PJ, Pierpaoli C. Microstructural and physiological features of tissues elucidated by quantitative-diffusion tensor MRI. *J Magn Reson B* 1996;111:209–19.
- [18] Ulug AM, van Zijl PC. Orientation-independent diffusion imaging without tensor diagonalization: anisotropy definitions based on physical attributes of the diffusion ellipsoid. *J Magn Reson Imaging* 1999;9:804–13.
- [19] Basser PJ, Pierpaoli, C. Elucidating tissue structure by diffusion tensor MRI. In: *Proceedings of SMR/ESMRMB Joint Meeting*, Nice, 1995. p. 900.
- [20] Papadakis NG, Xing D, Houston GC, et al. A study of rotationally invariant and symmetric indices of diffusion anisotropy. *Magn Reson Imaging* 1999;17:881–92.
- [21] Martin KM, Papadakis NG, Huang CL, et al. The reduction of the sorting bias in the eigenvalues of the diffusion tensor. *Magn Reson Imaging* 1999;17:893–90.
- [22] Bastin ME, Armitage PA, Marshall I. A theoretical study of the effect of experimental noise on the measurement of anisotropy in diffusion imaging. *Magn Reson Imaging* 1998;16:773–85.
- [23] Morse PM, Feshback H. *Method of theoretical physics*. McGraw Hill, 1953.
- [24] Cox RW, AFNI, software tools for analysis and visualization of functional magnetic resonance neuroimages. *Computer Biomed Res* 1996;29:162–73.
- [25] Cox RW, Hyde JS. Software tools for analysis and visualization of FMRI Data. *NMR Biomed* 1997;10:171–8.
- [26] Gold S, Christian B, Arndt S, et al. Functional MRI statistical software packages: a comparative analysis. *Human Brain Mapping* 1998;6:73–84.
- [27] Stejskal EO, Tanner JE. Spin diffusion measurements: spin echos in the presence of time-dependent field gradient. *J Phys Chem* 1965;42:288–92.